Polymer 53 (2012) 2394–2401

Contents lists available at SciVerse ScienceDirect

Polymer

journal homepage: www.elsevier.com/locate/polymer

Enhanced gas transport properties and molecular mobilities in nano-constrained poly[1-(trimethylsilyl)-1-propyne] membranes

Lakshmi S. Kocherlakota, Daniel B. Knorr Jr.[1], Laura Foster, René M. Overney*

Department of Chemical Engineering, University of Washington, Seattle, WA 98195, United States

ARTICLE INFO

Article history:
Received 30 December 2011
Received in revised form
28 March 2012
Accepted 31 March 2012
Available online 7 April 2012

Keywords:
PTMSP
Permeability
Ultrathin membranes

ABSTRACT

Interfacial constraints in ultrathin poly(l-trimethylsilyl-1-propyne) (PTMSP) membranes yielded gas permeabilities and CO_2/helium selectivities that exceed bulk PTMSP membrane transport properties by up to three-fold for membranes of submicrometer thickness. Maximum permeability coefficients of 110×10^3 Barrer and 27×10^3 Barrer for carbon dioxide and helium, respectively, were found to occur in membranes of ~750 nm thickness. Indicative of a free volume increase, a molecular energetic mobility analysis (involving intrinsic friction analysis) revealed enhanced methyl side group mobility. This was evidenced by a minimum in the activation energies of ~4 kcal/mol in thin PTMSP membranes with maximum permeation, compared to ~5.5 kcal/mol in bulk films. Aging studies conducted over the timescales relevant to the conducted experiments signify that the free volume states in the thin film membranes are highly unstable in the presence of sorbing gases such as CO_2. These results are discussed and contrasted to PTMSP bulk membrane systems, which were found to be unaffected by aging over the equivalent experimental time scale.

1. Introduction

Polymeric membranes are gaining wide attention in separation processes owing to their economic viability and operational flexibility [1,2]. Poly(l-trimethylsilyl-1-propyne)(PTMSP), a high free volume glassy polymer, exhibits extraordinarily high gas permeability coefficients and high organic-vapor/permanent-gas selectivities. These unusual transport properties in PTMSP are attributed to its high fractional free volume (FFV) of about 0.34 [3], caused by the inefficient chain packing involving rigid carbon–carbon double bonds, bulky trimethylsilyl and methyl constituent groups, coupled with poor inter-chain cohesion [4–6]. PTMSP has been shown to possess a bimodal distribution of small and large free volume elements with average sizes of 0.4 nm and 1.4 nm [7], which demands careful attention when choosing a transport model.

In dense polymeric membranes with free volume elements less than ~0.5 nm, molecular transport is driven by the concentration gradient of the penetrant across the membrane and is best described by the *solution diffusion model* [8]. In these membranes, the free volume elements exist as statistical fluctuations, appearing and disappearing at the same time scale, as gas molecule permeation through the membrane. According to this model, the gas permeability coefficient (P) is defined as,

$$P = DS, \tag{1}$$

where D and S are the gas diffusivity and solubility coefficient, respectively. As the selectivity of the gas component A over B is determined from the permeability ratio,

$$\alpha_{A/B} = \frac{P_A}{P_B} = \left(\frac{D_A}{D_B}\right)\left(\frac{S_A}{S_B}\right), \tag{2}$$

the transport is either diffusion or solubility dominated. If a membrane exhibits higher permeability to the larger molecular gas species, due to higher condensability compared to the smaller light gas counterpart, the process is often referred to as 'reverse selective' transport [9–11]. This applies to CO_2/helium transport through PTMSP, where the solubility ratio dominates [10], as CO_2 possesses a higher sorption coefficient in PTMSP than helium. In contrast, pressure driven *convective pore-like flow* transport mechanisms are found for mass transport systems with free volume elements that exceed ~1 nm in characteristic dimension, and are fixed in size and position relative to the time scale of permeant motion [8].

Owing to the presence of relatively large free volume elements, PTMSP emerges as a *transitional* polymer, with molecular transport occurring via a combination of convective permeation and solution

* Corresponding author.
E-mail address: roverney@u.washington.edu (R.M. Overney).
[1] Current address: Weapons and Materials Research Directorate, Materials and Manufacturing Science Division, Macromolecular Science and Technology Branch, United States Army Research Laboratory, Aberdeen Proving Ground, MD, USA.

0032-3861/$ – see front matter © 2012 Elsevier Ltd. All rights reserved.
doi:10.1016/j.polymer.2012.03.067

diffusion mechanisms [5,8,11]. Due to its high free volume, PTMSP behaves as an ultramicroporous membrane, with *interconnected microvoids* [12], resulting in pore flow dominated gas transport [5]. High reverse selectivities towards larger gas components in mixed gas transport were attributed to specific adsorption of the larger permeates within the walls of interconnected free volume elements, thereby creating resistance to transport of smaller, permeate gases [10]. PTMSP possesses a high glass transition temperature (T_g) in excess of 250 °C and degrades thermally before it reaches T_g [13].

Apart from its high gas permeability, PTMSP also exhibits unusual transport properties when subjected to external constraints, as found in the case of nanoparticle based composites [11,14–16]. For instance, Merkel et al. observed that gas permeabilities in PTMSP systematically increased with increased concentration of nanoscale, non-porous, fumed silica (FS) particles [11]. Converse results were obtained for the reverse selectivity. It was concluded that PTMSP's inefficient packing was further enhanced by the incorporation of FS nanoparticles, resulting in *free-phase-transport*, i.e., Knudsen diffusion, which positively impacts permeation but reduces reverse selectivity. Apart from the enhanced free volume, interstitial cavities (mesopores) were also observed to be formed due to particle aggregation in PTMSP nanocomposites leading to a decrease in selectivity [17]. Particle-polymer interaction effects on transport properties of nanocomposites were also investigated in PTMSP nanocomposite studies involving MgO and TiO_2 nanoparticles [14,15]. Both studies reveal increased gas permeabilities compared to bulk PTMSP for higher particle loadings (>7–10 nominal volume %) due to void generation caused by particle aggregation.

To obtain "particle aggregation free" access to interfacial properties, it has been shown that a planar confinement of thin films yields results quantitatively equivalent to those found in nanocomposites [18,19]. As planar arrangement imposes *uniform* interfacial confinement on the polymer matrix, it provides an interfacial system that can be analyzed more accurately without the complication of particle aggregation. In regards of the material studied here, this approach is well founded, considering the low interfacial interaction (~100 mJ/m) between PTMSP and SiO_2 [20]. In the study presented here, we compare the transport properties of free standing thin film PTMSP membranes with the thermo-mechanical properties of SiO_2 supported thin PTMSP films to probe the effect of molecular relaxations on interfacially imposed transport alterations. This involved the systematic analysis of CO_2 and helium permeabilities as a function of the membrane thickness, and measurement of local molecular mobilities that were extracted from nano-thermo-mechanical probing.

2. Experimental section

PTMSP (SSP-070-10gm, lot 9H-15058 Gelest, Inc.) was dissolved in cyclohexane (SSP 4878-02, lot H07623 & G38629, Mallinckrodt Chemicals) at room temperature, producing solutions of concentrations varying from 0.3 to 1.0 wt.% that were subsequently filtered with a 0.2 μm Nylon (Whatman) filter. Anodic aluminum oxide (AAO) membranes (Anodisc 13, 0.2 μm, Whatman, Inc.), which served as supports for PTMSP films, were attached to aluminum discs with 3 mm holes in the center via an epoxy (5 Minute®, Devcon), exposing the sample area for gas permeation. These membranes were dried for 24 h before the PTMSP films were spin coated to ensure complete curing of the epoxy, thus preventing any possible contamination of the films. Furthermore, these aluminum discs with the AAO membranes were attached to the silicon substrate during spin casting to prevent both direct exposure to vacuum on the spin chuck (that holds the sample in place) and possible infiltration of the PTMSP solution into the pores of the AAO membranes. Films of different thicknesses were prepared by spin casting 100 μL of the PTMSP solution at speeds varying from 1000 rpm to 6000 rpm for 1 min on 200 nm pore AAO membranes. Thicker films were fabricated either by solution casting or by spin casting multiple layers of PTMSP to build up the thickness. A cross-sectional view of the spin casted PTMSP membranes for gas permeation measurements is shown in Fig. 1. For IFA measurements, samples ranging in thickness from 200 nm to 1.4 μm were prepared by spin casting 1.0 and 2.0 wt.% PTMSP solutions on <1,1,1> silicon wafers pre-cleaned by sonication in acetone (10 min) followed by methanol (40 min), and then UV/ozone cleaning (UV/Ozone, Bioforce) for 20 min. All the films were dried under ambient conditions. Thin PTMSP films were dried for 18–20 h, while the thicker films (>1 μm) were dried for about 36 h.

Permeability measurements were performed using an isobaric permeation system, with regulated gas flow feed to the upstream side of the membrane while the downstream side was maintained at atmospheric pressure. A purge valve was used to vent the gas and remove any contaminant gases present in the line. The downstream permeate gas flow rate (dV/dt) was determined using a bubble flow meter. For each upstream gas pressure (p_2), measurements were repeated until a steady state in the permeate gas flow rate was observed, which was then recorded. The observed average time to reach steady state was about 5–10 min. The downstream pressure (p_1) was maintained at atmospheric pressure for all the experiments. The gas permeability, P (1 Barrer = 10^{-10} (cm^3(STP) cm)/(cm^2 s cmHg) was determined from the flux, J (cm^3(STP)/cm^2 s), the membrane cross-sectional area, A (cm^2), the thickness, l (cm), and the externally controlled differential pressure, Δp ($\Delta p = p_2 - p_1$), (cmHg) as:

$$P = \left(\frac{Jl}{\Delta p}\right) \tag{3}$$

Flux was obtained from the following expression [10]

$$J = \left(\frac{273.15 p_{atm}}{76T}\right) \frac{1}{A}\frac{dV}{dt} \tag{4}$$

where p_{atm} is the atmospheric pressure in cmHg, T is the temperature of the gas in Kelvin, (dV/dt) is the gas flow rate in cm^3/s. Membrane thicknesses were measured by contact mode scanning force microscopy (SFM) (*Easy Scan 2*, Nanosurf GmbH) of a scratch made on the PTMSP surface penetrating the thickness of the polymeric film, avoiding perturbing/damaging the supporting AAO membrane after the gas permeabilities had been measured. Gas permeation behaviors were measured in two ways: (i) the initial gas analyzed was CO_2 followed by helium on neat PTMSP films on a series of samples with thicknesses between 200 nm and 4 μm, (ii) the order of the permeates was reversed, i.e., the membranes were exposed first to helium and then to CO_2, and for this measurement a new set of neat membranes were used.

Local energetic investigations were performed on PTMSP thin film samples on silicon wafers with intrinsic friction analysis (IFA) involving contact SFM (*Explorer*, Veeco Inc.) with a custom heating stage. IFA, as described in detail elsewhere [21,22], is a spectroscopic contact mode SFM method that is highly surface sensitive. It

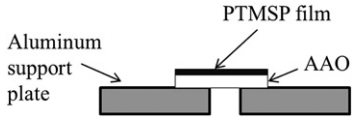

Fig. 1. Cross-sectional view of PTMSP film sample spin casted on AAO over the aluminum support with center hole (diameter 3 mm) for gas permeation.

provides energetic information about the thermally active modes, such as molecular and sub-molecular mobilities. Briefly, the friction force is determined from the hysteresis in the torsional cantilever deflection between forward and reverse scans. To deduce the apparent activation energy of the segmental motion, friction force isotherms are obtained by varying scanning velocities for various constant temperatures. These isotherms are superimposed to an arbitrary reference isotherm by shifting them with horizontal distances $\ln(a_T)$, where a_T is the thermal shift factor, based on the widely known time–temperature superposition principle [23,24]. The apparent activation energy is deduced from $\ln(a_T)$ plots as a function of reciprocal absolute temperature.

Lateral force measurements over a 1 μm scan range were performed at temperatures ranging from 30 to 114 °C. Levers (PPP-CONT, Nanosensors) with nominal and lateral spring constants of ~0.2 N/m and 80 N/m, respectively were used. Prior to the experiment, the levers were conditioned and calibrated. Conditioning of the cantilever tip and calibration of the cantilever torsional spring constant involved pre-scanning on well prepared silicon wafers [22,25]. Tip conditioning involved two steps: (1) chemical-mechanical polishing of the tip on the silicon wafer, and (2) surface passivation of the polished tip surface with the material to be investigated (i.e., PTMSP). In the course of the conditioning process, which eliminates sharp tip asperities, the torsional spring constant is obtained via a blind calibration [25]. All the IFA studies were performed in a glove box with a dry nitrogen atmosphere (<10% humidity).

3. Results and discussion

With 757 nm and 4 μm thick PTMSP films, two representative film thickness regimes are contrasted relative to their CO_2 permeation properties as a function of the pressure drop ($\Delta p = p_2 - p_1$) across the membrane, Fig. 2. These data are compared to permeability coefficients provided by Srinivasan et al. [5], involving significantly thicker "bulk" PTMSP membranes (~100 μm) that show, as expected, a decrease in the permeability of sorbing gases in glassy polymers with increasing gas pressure, Δp [5,26].

Gas transport in glassy polymeric systems is frequently described in terms of a *dual mode sorption* (DMS) *model* [26,27], i.e.,

$$P = k_D D_D + \frac{C_H b D_H}{(1 + bp_1)(1 + bp_2)} \quad (5)$$

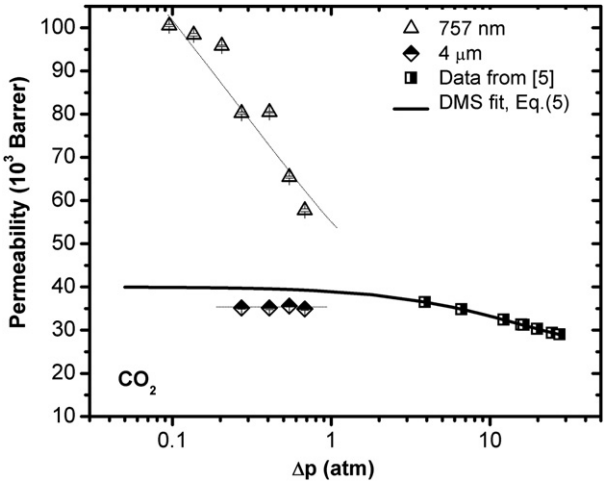

Fig. 2. Comparison of CO_2 permeability coefficients as function of the pressure drop, Δp, of relatively thick (4 μm) and ultrathin (757 nm) films with bulk (115 μm) membrane data [5], that serve as the basis for the DMS model extrapolation (solid line).

that relates the total permeability P to the membrane's upstream and downstream pressures, p_2 and p_1, respectively. The first term on the right-hand side in Eq. (5), which is reflective of the gas permeation through a densified polymer matrix, represents the product of the Henry's law solubility parameter, k_D, and the penetrant diffusion coefficient, D_D. The second term, containing the Langmuir sorption capacity parameter C_H, the affinity parameter b, and the diffusion coefficient through the Langmuir sites D_H, takes account of the permeation through the excess free volume elements in the polymeric matrix. Applying the DMS model to Srinivasan et al.'s data set, and extrapolating it towards low pressures, Fig. 2, reveals a reasonable correspondence with our 4 μm data set. The thinner films (represented by the 757 nm film), however, do not conform to the DMS bulk membrane model, neither regarding the permeation magnitude that reveals unexpectedly high permeabilities at low pressure drops, nor its gradient. While we will argue in this paper that the observed enhancement in gas permeation originates from finite size constraints acting on the polymer matrix, the strong dependence of the permeability on pressure will be shown to be caused by accelerated aging of ultrathin PTMSP films when exposed to CO_2.

The impact of aging on the permeation properties of PTMSP for the sorbing gas, CO_2, and the non-sorbing gas, helium, is documented in Fig. 3(a,b). Ultrathin polymer membranes are known to exhibit accelerated aging that is caused in part by both the non-equilibrium nature of interfacially constrained systems [28–30], and the plasticizing effect of sorbing permeates in glassy polymers [31]. We found for relatively thick films (>1 μm), Fig. 3(a), the CO_2 permeability coefficient initially increases and then saturates at 36×10^3 Barrer; this corresponds well to the performance of bulk membranes (see Fig. 2). The increase in permeability of CO_2 in micrometer thick PTMSP membranes, as shown in Fig. 3(a), originates from plasticization effects caused by strongly sorbing gases like CO_2. Similar time dependent CO_2 permeation behaviors have been widely observed in a variety of glassy polymers [32,33]. Over the time scale of observation, our micrometer thick membranes did not exhibit physical aging, which is apparent from the constant permeability coefficient of $\sim 36 \times 10^3$ Barrer, which was maintained up to 10 h, a time scale that is relevant for the thin film study presented here. In contrast to CO_2, helium transport, measured through another fresh membrane of similar thickness without prior CO_2 exposure, revealed, over the same time period, a steady permeability coefficient (as anticipated from a non-sorbing gas) of around 6×10^3 Barrer, Fig. 3(a).

For ultrathin films (<1 μm), Fig. 3(b), the initial increase (sorption period) in CO_2 permeability is, as expected, much faster than that of thicker films. Extremely high maxima in permeability coefficients of 90×10^3 and 19×10^3 Barrer for CO_2 and helium, respectively, are observed. These values are almost three times the bulk permeation values, and are indicative of increased free volume in interfacially constrained ultrathin films. The sharp drop in CO_2 permeability is an indication of accelerated aging in thin PTMSP films that dominates the plasticization effect in the polymer caused by the sorbing gas, an argument that has also been made for ultrathin Matrimid™ films, although over a longer time period [31]. It can be assumed that local confinement effects (i.e., thin film confinement) imposed by interfacial constraints in thin PTMSP films are affected much more rapidly by plasticizing effects of CO_2, leading to accelerated aging. Along this line, it has to be noted for future reference that, if physical aging were suppressible, an even higher permeation maximum could have been expected. Helium also revealed a permeability reduction in ultrathin PTMSP films from 19×10^3 Barrer to 6×10^3 Barrer, Fig. 3(b), although the rate of aging is significantly lower than that of CO_2. The reduction in helium permeability over time indicates that thin PTMSP films also

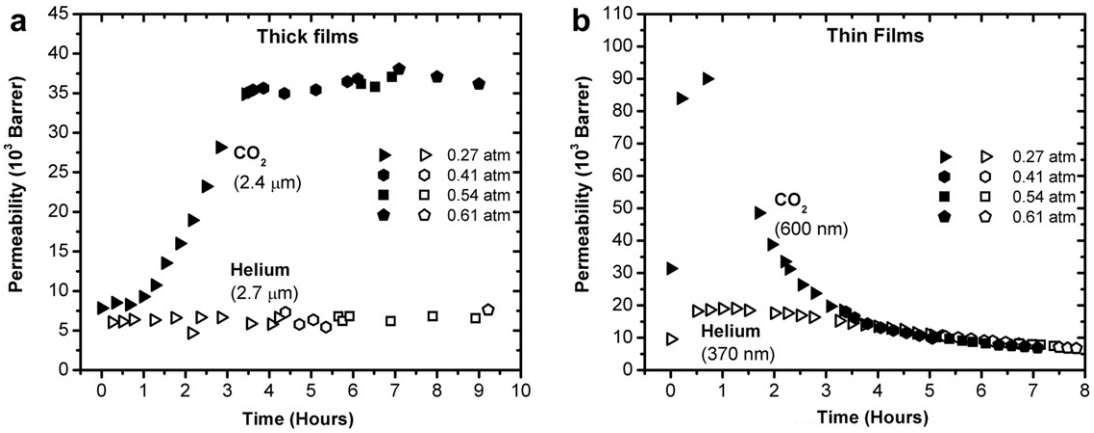

Fig. 3. Temporal development of CO_2 and helium permeability coefficients in (a) thick PTMSP membranes (2.4 μm and 2.7 μm) and (b) thin films (600 nm and 370 nm) are shown, for differential pressures varying from 0.27 to 0.61 atm. CO_2 permeability coefficients are represented by filled symbols and those of helium with open (unfilled) symbols.

undergo physical aging without the influence of conditioning effects, such as those caused by the presence of sorbing gases like CO_2.

Having addressed the impact of aging, which, for ultrathin films is driven by non-equilibrium free volume relaxation modes, and is further accelerated in the presence of a strongly sorbing gas, we are now ready to present and discuss PTMSP thin film permeation properties. In Fig. 4(a,b), the CO_2 and helium permeability coefficients are compiled for 240 nm to 4 μm thick PTMSP membranes. The permeability coefficients of CO_2 and helium shown in Fig. 4(a,b) were all evaluated at low pressure drops ($\Delta p = 0.2$ atm) for consistency, even though the helium permeation was largely independent of the pressure drop applied across the membrane. The plots in Fig. 4 reveal non-monotonous permeation vs. thickness functional behavior for both CO_2 and helium in the sub-micron regime, while films thicker than ~1.5 μm show permeability coefficients coinciding with bulk values of 36×10^3 Barrer and 6×10^3 Barrer for CO_2 and helium, respectively. Permeation maxima are observed at around 750 nm. It is important to note that the helium permeation measurements in Fig. 4(b) involved PTMSP films that have not been previously exposed to CO_2. To warrant time invariant comparisons, it is to be noted that the permeability coefficients of CO_2 for the investigated thick films (>1 μm) were all recorded 3 h after the exposure to CO_2, i.e., when steady state values could be obtained for the permeability coefficients over the timeframe of the experiment, as shown in Fig. 3(a). For thin films, the exposure time was restricted to 15–30 min before recording the permeability coefficients to reduce the associated aging effects, as shown in Fig. 3(b). Furthermore, all the measurements in thin films were completed within 2 h. The permeability coefficients of helium were obtained after 30 min of gas (helium) permeation for both the thick and thin films, and the measurements were taken within 2 h of gas exposure time for consistency. To ensure that the bulk deviating transport properties in the 600–750 nm films were not a consequence of polymeric impregnation into the pores of the supporting AAO membranes, we determined bulk equivalent thicknesses, that is, $l_{bulk} = P\Delta p/J$. Thereby, we assumed bulk permeation behavior of CO_2 (i.e., $P = 35 \times 10^3$ Barrer [5]), and substituted for the measured Δp and J (the permeation data of 600–750 nm films shown in Fig. 4). The resulting equivalent thicknesses, l_{bulk}, significantly underestimate the PTMSP film thicknesses on AAO determined by SFM ($l_{bulk} \approx 260$ nm for $\Delta p = 0.27$ atm and $J = 2.745$ cm^3(STP)/cm^2 s for an SFM determined film thickness of 600–750 nm), confirming no PTMSP impregnation into AAO.

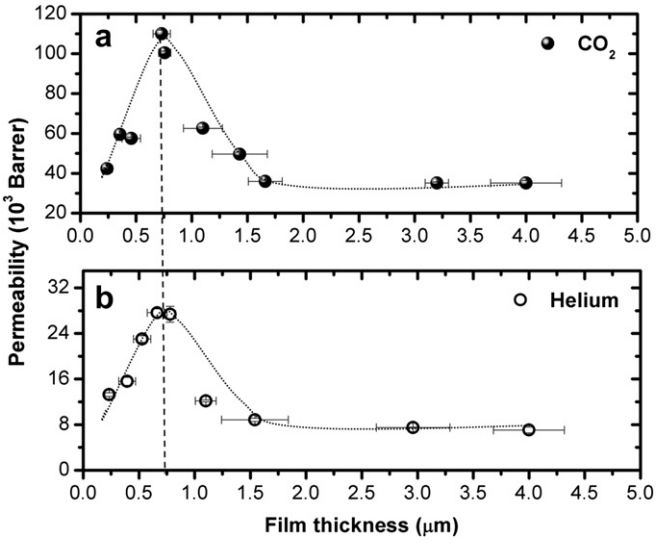

Fig. 4. Permeability coefficients of (a) CO_2 and (b) helium, as function of film thickness. A maximum in the permeation behavior is observed at film thicknesses of 600–750 nm for both gases.

To provide an explanation for the non-monotonous permeation behavior of PTMSP in the thin film region, we conducted an energetic molecular relaxation mobility analysis based on intrinsic friction analysis (IFA) [21,22,34,35]. The IFA methodology, as described in the experimental section, has been shown to be a reliable spectroscopic method to extract energetic molecular mobility information from thin polymer systems. It is important to note that the activation energies obtained by IFA are not diffusion activation energies, but activation energies related to molecular relaxation. In Fig. 5(a), a representative IFA friction-velocity master curve for an 860 nm thick PTMSP film on silicon oxide is shown, revealing in the inset of Fig. 5(a) an activation energy of 5.6 ± 0.2 kcal/mol. From similar friction-velocity data sets, activation energies from 200 to 1400 nm thick PTMSP films could be determined, as compiled in Fig. 5(b). The activation energies were found to vary from 4 to 7 kcal/mol, depending on the film thickness. In the thick film regime (>1 μm), the activation energy is 5.4 ± 0.3 kcal/mol, which can be attributed to the rotation of the methyl groups on the PTMSP backbone [36], the only mode that is thermally active, as per molecular conformational calculations

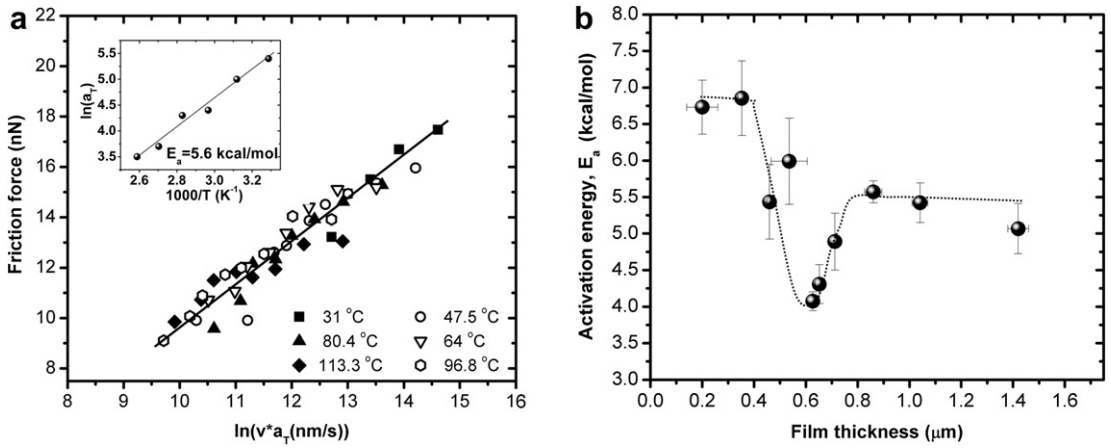

Fig. 5. Activation energies in PTMSP obtained from IFA. (a) Representative IFA master curve for 860 nm thick PTMSP film over a temperature range from 31 °C to 113 °C, revealing an activation energy of $E_a = 5.6$ kcal/mol (inset), attributed to the methyl side group rotation. (b) Enthalpic (activation) energies of the methyl side group rotation for film thicknesses between 200 and 1400 nm.

[36]. Changes in the activation energies associated to the thermally active modes allow us to draw inferences about how the confinement affects the state of the polymer. The minimum in the activation energy of 4.0 kcal/mol at 600–650 nm in Fig. 5(b) signifies a maximum in the local rotational mobility of the methyl groups. This coincides with the CO_2 and helium permeation maxima observed in thin film membranes, as shown in Fig. 4. The link made here between molecular mobility and gas transport involving glassy polymers finds support in other studies, such as the quasi-elastic neutron scattering study by Kanaya et al., in which a linear relationship was observed between the oxygen diffusion coefficient and local side-chain molecular mobilities in polyacetylenes [37].

The three IFA identified thickness (t) regimes can be interpreted as follows:

- $t < 300$ nm: In the ultrathin film regime, the observed higher activation energies indicate restricted molecular mobilities, representative of interfacial molecular alignment with increased packing densities, as reported, for instance, by van der Lee et al. for thin PMMA films [38], although it should be noted that these observations occurred in thinner films. This is not surprising as PMMA is much more flexible than the highly rigid PTMSP molecules.
- $t > 800$ nm: In the thick (bulk-like) film regime, the activation energy saturates to a constant value, indicative of bulk-like polymeric structural properties.
- 300 nm $< t <$ 800 nm: The local and temporal anisotropy of polymer packing and relaxation acts as the driving force for "autodiffusion" [39,40], i.e., interdiffusion of the polymeric chains during the naturally occurring temporal annealing process, when the solvent is driven out. Paired with the inflexibility of PTMSP's rigid backbone, a loosely packed polymeric phase is established within the intermediate film thickness region. Thus, the observed minimum activation energies in Fig. 5(b) at 600–650 nm, which reveal maximum molecular side-chain mobilities, originate from higher free volume in the polymer phase. This is in agreement with permeation and free volume studies involving SiO_x/PTMSP nanocomposites that report enhanced free volume within the polymer phase, and suggest the presence of interconnected channels [11]. The observed maximum in gas permeabilities (Fig. 4) for film thicknesses of ~750 nm also supports the argument of high free volume in the polymeric phase. The apparent delay to reach bulk permeation properties at ~1.5 μm compared to the mobility analysis at ~800 nm film thickness is due to the integral effect of permeation measurements.

Although the large length scales over which interfacial constraints affect the polymer matrix are at first sight astonishing, they have been observed in the literature for rigid polymeric systems, such as conjugated polymers [41]. Polymer chain flexibility and inter-chain cohesive energies were found to have strong influence on the free volume and transport properties in glassy polymers [4,6].

Since this study addresses only single component gas transport, we have to differentiate the order in which gases flow through the membrane. For this purpose, we present in Fig. 6, CO_2 and helium permeability coefficient data involving ultrathin (663 and 757 nm) and thick (1.43 and 1.54 μm) membranes that were exposed to both gases in different orders. One film of each mentioned film thickness pair was first exposed to helium, i.e., 663 nm and 1.54 μm thick films (filled symbols), followed by CO_2 permeation. The order was reversed for films of thickness 757 nm and 1.43 μm (open symbols), wherein the films were exposed to CO_2 first. It can be seen from Fig. 6(a), that the CO_2 transport is essentially unaffected by any preceding helium exposure, regardless of the film thickness. This is expected, as helium, a light permeate gas, has low condensability in PTMSP and hence does not alter the polymeric matrix. A corresponding result was also found for helium; that is, helium permeation through thick films did not depend on prior CO_2 transport, Fig. 6(b). The findings are different, however for helium permeation in the ultrathin film regime, where the permeation coefficients depend on the membrane CO_2 history, Fig. 6(b). In the ultrathin film regime, i.e., the 663 nm thick PTMSP membrane, which was first purged with helium, ultra-high helium permeabilities around 28×10^3 to 30×10^3 Barrer were found. These values differ significantly from the helium permeation after CO_2 exposure, which was around 9×10^3 to 10×10^3 Barrer, as found for the 757 nm film in Fig. 6(b). This indicates that CO_2 permeation results in accelerated aging for ultrathin films, an aspect we addressed earlier, Fig. 3(b), and discussed in terms of a reduction in the overall free volume. Once again the total timeframe of exposure to CO_2 in the case of thin films was restricted to less than 2 h, while the thick film data were collected after steady state values were achieved, as discussed above in the context of Figures 3 and 4. Helium permeation data was also collected in the same timeframe as discussed above for both thick and thin films.

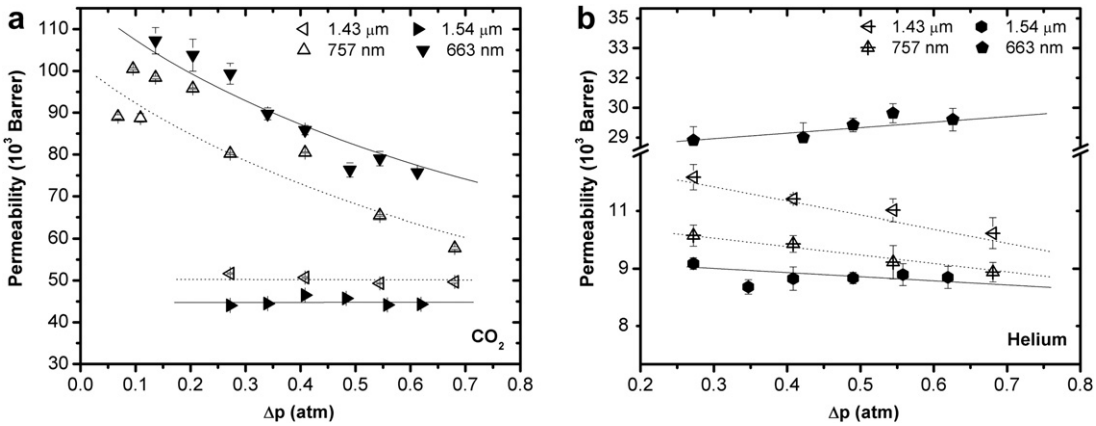

Fig. 6. Comparison of (a) CO_2 and (b) helium permeability coefficients of ultrathin (663 and 757 nm) and thick (1.43 and 1.54 μm) PTMSP membranes, exposed initially either to helium (663 nm and 1.54 μm) or CO_2 (757 nm or 1.43 μm). Filled symbols and solid guiding lines in Fig. 6(a and b) represent films that were exposed to helium first. Open symbol data points and dotted guiding lines represent films exposed to CO_2 first.

The impact of CO_2 permeation and interfacial constraints on physical aging in PTMSP and helium permeation is illustrated in Fig. 7(a,b) for thick and thin film systems. The schematic represents a simplified visualization of the interplay between the pore distribution and transport properties of PTMSP before and after CO_2 exposure. Bulk PTMSP films possess a distribution of small and large pores (cavity sizes of about 0.4–0.5 nm and 0.75–1.4 nm, respectively [7,42]). Our results indicate that, in thin films (<1 μm) prior to CO_2 exposure, helium experiences less resistance to flow, evidenced as higher gas permeabilities, suggesting enhanced free volume. However, when exposed to CO_2, which yields an accelerated physical aging effect in thin films, the free volume elements shrink (collapse) resulting in a decrease of the helium flux, as shown on the right of Fig. 7(a). On the other hand, in thicker PTMSP films, where interfacial effects are lost, and thus, the free volume elements are smaller than those in ultrathin films, aging effects over the same (short) time scale of ~10 h are significantly less prominent, leaving the helium transport indifferent to the membrane CO_2 history, Fig. 7(b). It is to be noted that the schematic in Fig. 7 is only a simplified depiction of a possible impact of CO_2 permeation on the polymer matrix, and does not capture all the probable scenarios that can affect the free volume distribution in the polymeric matrix or the transport properties. For instance, CO_2 plasticization can induce physical aging leading to pore collapse of larger pores, and thus, a decrease in the number of pores, as well as a decrease in the size of the small pores [42].

Finally, we turn our attention to the resulting CO_2/helium selectivity of thin PTMSP membranes, based on data presented above. The "reverse selectivity" of CO_2 over helium, i.e., ($\alpha_{CO_2/He} = P_{CO_2}/P_{He}$) is presented in Fig. 8, for both gas flow order scenarios. Monotonous enhancement in reverse selectivity was observed with decreasing film thickness in films exposed to CO_2 first. Thicker films (>1 μm) exhibit $\alpha_{CO_2/He}$ values between 5 and 6, corresponding well to the literature [5,10]. Thin films, such as the 240 nm films, however, reveal remarkably high values of up to 17. Note that the aging effect caused by CO_2 in thin films (discussed with Figs. 3 and 6(b)) is also pertinent to mixed gas permeabilities, and is

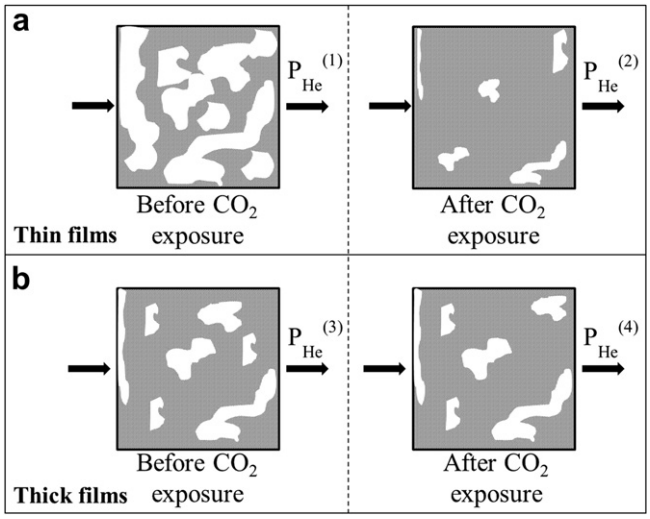

Fig. 7. Simplified schematic representation of the free volume alterations and the corresponding helium permeation, P_{He}, involving to part CO_2 exposure and interfacial constraints, shown for (a) thin films and (b) thick bulk-like membranes. The magnitudes of permeation, $P_{He}^{(1)} > P_{He}^{(3)} \geq P_{He}^{(4)} > P_{He}^{(2)}$, are in coordination with the sketched free volumes.

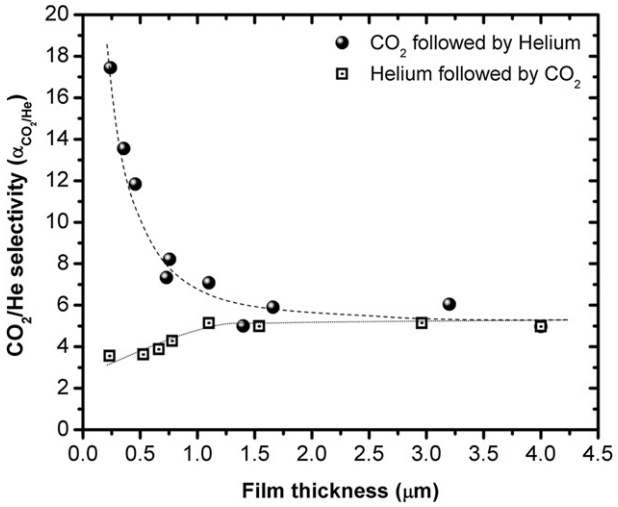

Fig. 8. CO_2/helium selectivity in PTMSP as function of film thickness reported in two different orders: (i) Films purged first with CO_2 followed by helium. (ii) Films purged first with helium followed by CO_2. The reverse selectivities shown in both the scenarios were obtained at $\Delta p = 0.2$ atm.

overemphasized in this study by exposing the membrane to a 100% CO_2 gas stream before exposing it to helium.

Enhanced selectivities of condensable gases over light gases through thick PTMSP membranes were already reported earlier, in the case of mixed gas permeation [10]. Selectivity enhancements were attributed to the partial blocking of the free volume elements by the condensable gas component, causing a hindrance to the flow of the light gas component in the gas mixture. It is important to note that, in mixed gas studies [10], the light gas component permeabilities were considerably lower in comparison to single component gas permeation values, but, the condensable gas component permeabilities remained unaltered. Similar behavior was also evident here for CO_2 in both thick and ultrathin films, Fig. 6(a). Based on our single gas permeation results presented here, we argue that mixed gas studies of CO_2/helium involving ultrathin films would result in a further enhancement of the CO_2/helium selectivity. This argument is based on (i) the simultaneous blocking effect towards helium permeation due to the co-permeation of the strongly sorbing gas CO_2, as well as, (ii) the strong plasticization effects of CO_2 found in confined ultrathin films. An opposite trend in selectivity is observed for ultrathin film systems if purged first with helium, also shown in Fig. 8, as expected from the high permeation values of helium in the ultrathin film region, Fig. 6(b).

4. Conclusion and summary

Interfacial constraints in ultrathin PTMSP membranes resulted in structural adaptations in the polymer matrix that gave rise to enhanced gas permeabilities and bulk deviating CO_2/helium selectivities. Gas transport properties of PTMSP, analyzed as function of the membrane thickness, revealed a non-monotonous gas permeation behavior of CO_2 and helium, with an approximate three-fold enhancement than bulk values for thin film membranes of ~750 nm thickness. Based on the thickness dependent molecular mobility analysis of thermally active modes in PTMSP, we can conclude that the interfacially induced structural adaptations in PTMSP lead to an increase in free volume for films of 400 to 800 nm thickness. This termination is based on the mobility enhancement found in the methyl side groups within this film thickness regime. However, our aging analysis revealed that these “free-standing” ultrathin membrane films physically age within hours due to the plasticizing effect of the sorbing gas component that causes a free volume collapse.

It is important to note that the membranes discussed here possess merely air–polymer interfaces. Thus, it could be argued that, in the presence of solid interfaces (as in nanocomposites), the polymer high free volume phase could be stabilized by stronger interfacial constraints. This would, however, require an appropriately high loading density of nanoparticles, to confine the polymer to regions of critical length scales. As discussed for PTMSP, the length scale is around 400 to 800 nm. The problem for PTMSP is that it is notoriously difficult to blend with nanoparticles such as silicon oxides due to particle aggregation, resulting in void generation for high particle loadings [14,15]. The formation of voids in nanocomposite membranes gives rise to alternate gas transport modes such as Knudsen flow, masking diffusive transport properties [14].

Considering that interfacial effects were found to impact material and transport properties for many polymer systems, such as the glass transition [39,43,44], relaxation [28,29] and gas transport properties [45], the findings presented here have wider implications. For PTMSP nanocomposites, solutions have to be found to capitalize on the interfacial polymer region surrounding the particles without jeopardizing the permeation properties by particle aggregation at high particle loading density. Furthermore, other materials with less impressive gas transport properties than PTMSP might provide comparable properties to bulk PTMSP but with high temporal stability, if interfacially constrained. That said, our on-going research focuses on the IFA screening of thin film membrane materials on functionalized and unfunctionalized inorganic surfaces for, the establishment of critical length scales that lead to increased free volume, and its translation to nanocomposite membranes.

Acknowledgments

This work was supported by the National Science Foundation (CBET 0729849). We thank Peggy Widjaja and Thao Nguyen for experimental assistance concerning IFA and the permeation flux analysis.

References

[1] Bernardo P, Drioli E, Golemme G. Industrial & Engineering Chemistry Research 2009;48(10):4638–63.
[2] Shao L, Low BT, Chung TS, Greenberg AR. Journal of Membrane Science 2009; 327(1–2):18–31.
[3] Morisato A, Shen HC, Sankar SS, Freeman BD, Pinnau I, Casillas CG. Journal of Polymer Science Part B-Polymer Physics 1996;34(13):2209–22.
[4] Nagai K, Masuda T, Nakagawa T, Freeman BD, Pinnau I. Progress in Polymer Science 2001;26(5):721–98.
[5] Srinivasan R, Auvil SR, Burban PM. Journal of Membrane Science 1994; 86(1–2):67–86.
[6] Savoca AC, Surnamer AD, Tien CF. Macromolecules 1993;26(23):6211–6.
[7] Hill AJ, Freeman BD, Jaffe M, Merkel TC, Pinnau I. Journal of Molecular Structure 2005;739(1–3):173–8.
[8] Wijmans JG, Baker RW. Journal of Membrane Science 1995;107(1–2): 1–21.
[9] Merkel TC, Freeman BD, Spontak RJ, He Z, Pinnau I, Meakin P, et al. Science 2002;296(5567):519–22.
[10] Pinnau I, Toy LG. Journal of Membrane Science 1996;116(2):199–209.
[11] Merkel TC, He ZJ, Pinnau I, Freeman BD, Meakin P, Hill AJ. Macromolecules 2003;36(18):6844–55.
[12] Hofmann D, Fritz L, Ulbrich J, Paul D. Polymer 1997;38(25):6145–55.
[13] Ichiraku Y, Stern SA, Nakagawa T. Journal of Membrane Science 1987;34(1): 5–18.
[14] Matteucci S, Kusuma VA, Kelman SD, Freeman BD. Polymer 2008;49(6): 1659–75.
[15] Matteucci S, Kusuma VA, Sanders D, Swinnea S, Freeman BD. Journal of Membrane Science 2008;307(2):196–217.
[16] Winberg P, Desitter K, Dotremont C, Mullens S, Vankelecom IFJ, Maurer FHJ. Macromolecules 2005;38(9):3776–82.
[17] De Sitter K, Winberg P, D'Haen J, Dotremont C, Leysen R, Martens JA, et al. Journal of Membrane Science 2006;278(1–2):83–91.
[18] Bansal A, Yang HC, Li CZ, Cho KW, Benicewicz BC, Kumar SK, et al. Nature Materials 2005;4(9):693–8.
[19] Sen S, Xie Y, Bansal A, Yang H, Cho K, Schadler LS, et al. European Physical Journal-Special Topics 2007;141:161–5.
[20] Killgore JP, Overney RM. Langmuir 2008;24(7):3446–51.
[21] Knorr DB, Gray TO, Overney RM. Journal of Chemical Physics 2008;129(7): 074504.
[22] Knorr DB, Gray TO, Overney RM. Ultramicroscopy 2009;109(8):991–1000.
[23] Ward IM. Mechanical properties of solid polymers. London: Wiley-Interscience; 1971.
[24] Ferry JD. Viscoelastic properties of polymers. John Wiley &Sons; 1980.
[25] Buenviaje CK, G SR, Rafailovich MH, Overney RM. Atomic force microscopy calibration methods for lateral force, elasticity, and viscosity. Materials Research Society Symposium Proceedings 1998;552:187–92.
[26] Merkel TC, Bondar V, Nagai K, Freeman BD. Journal of Polymer Science Part B-Polymer Physics 2000;38(2):273–96.
[27] Koros WJ, Chan AH, Paul DR. Journal of Membrane Science 1977;2(2): 165–90.
[28] Rowe BW, Freeman BD, Paul DR. Polymer 2009;50(23):5565–75.
[29] Huang Y, Paul DR. Polymer 2004;45(25):8377–93.
[30] Dorkenoo KD, Pfromm PH. Macromolecules 2000;33(10):3747–51.
[31] Horn NR, Paul DR. Polymer 2011;52(7):1619–27.
[32] Bos A, Punt IGM, Wessling M, Strathmann H. Journal of Polymer Science Part B-Polymer Physics 1998;36(9):1547–56.
[33] Kanehashi S, Nakagawa T, Nagai K, Duthie X, Kentish S, Stevens G. Journal of Membrane Science 2007;298(1–2):147–55.
[34] Sills S, Overney RM. Physical Review Letters 2003;91(9).
[35] Sills S, Gray T, Overney RM. Journal of Chemical Physics 2005;123(13).

[36] Knorr DB, Kocherlakota LS, Overney RM. Journal of Membrane Science 2010; 346(2):302–9.
[37] Kanaya T, Tsukushi I, Kaji K, Sakaguchi T, Kwak G, Masuda T. Macromolecules 2002;35(14):5559–64.
[38] van der Lee A, Hamon L, Holl Y, Grohens Y. Langmuir 2001;17(24):7664–9.
[39] Sills S, Overney RM, Chau W, Lee VY, Miller RD, Frommer J. Journal of Chemical Physics 2004;120(11):5334–8.
[40] Buenviaje C, Ge SR, Rafailovich M, Sokolov J, Drake JM, Overney RM. Langmuir 1999;15(19):6446–50.
[41] Campoy-Quiles M, Sims M, Etchegoin PG, Bradley DDC. Macromolecules 2006; 39(22):7673–80.
[42] Consolati G, Genco I, Pegoraro M, Zanderighi L. Journal of Polymer Science Part B-Polymer Physics 1996;34(2):357–67.
[43] Forrest JA, Dalnoki-Veress K. Advances in Colloid and Interface Science 2001; 94(1–3):167–96.
[44] Keddie JL, Jones RAL, Cory RA. Europhysics Letters 1994;27(1):59–64.
[45] Killgore JP, Kocherlakota LS, Overney RM. Journal of Polymer Science Part B-Polymer Physics 2010;48(4):434–41.